INSTITUTE OF PHYSICS PUBLISHING JOURNAL OF PHYSICS B: ATOMIC, MOLECULAR AND OPTICAL PHYSICS

J. Phys. B: At. Mol. Opt. Phys. **39** (2006) 4179–4190 doi:10.1088/0953-4075/39/20/016

Benchmark experiment and theory for near-threshold excitation of helium by electron impact

Michael Lange[1], Jun Matsumoto[1], Julian Lower[1], Stephen Buckman[1], Oleg Zatsarinny[2], Klaus Bartschat[2], Igor Bray[3] and Dmitry Fursa[3]

[1] Centre for Antimatter-Matter Studies, Research School of Physical Sciences and Engineering, Australian National University, Canberra, Australia
[2] Physics Department, Drake University, Des Moines, IA, USA
[3] Centre for Antimatter-Matter Studies, Murdoch University, Western Australia, Australia

Received 24 July 2006, in final form 21 August 2006
Published 10 October 2006
Online at stacks.iop.org/JPhysB/39/4179

Abstract

A new experimental technique has been applied to measure absolute scattering cross sections for electron impact excitation of the $n = 2, 3$ states of helium at near-threshold energies. The experimental results are compared with predictions from recent state-of-the-art theoretical calculations. The calculations are performed using the R-matrix with pseudostates, B-spline R-matrix, and the convergent close-coupling methods. Generally, very good agreement is found between the experiment and the three theories.

1. Introduction

For electron–atom (molecule) scattering, the near-threshold regime, within a few electron volts of the lowest electronic excitation thresholds, is an interesting and challenging one for both experiment and theory. It is a complex region where, in many cases, the scattering process is dominated by short-lived, excited negative ions (negative ion resonances) where the projectile electron binds in a transient fashion to the target for a short period of time ($\sim 10^{-14}$–10^{-12} s). Studies in this regime require sophisticated experimental approaches and complex, coupled-channel calculations for a successful description of the scattering process.

This region is a challenge experimentally as measurements typically require stable, high-resolution electron monochromators and analysers, as well as a sound strategy for establishing the absolute magnitude of the scattering cross sections. For angular differential scattering measurements, the most commonly used approach has been to measure the flux of inelastically scattered electrons, for a particular scattering channel and scattering angle, relative to that for the elastic scattering intensity at the same incident energy and scattering angle. For most atoms and molecules that are gaseous at room temperature, the elastic scattering cross sections are now reasonably well established through the use of the relative flow technique (see, for example, Brunger and Buckman (2002)). Hence, if the transmission of the energy analysing device is known, the inelastic scattering cross section can be readily determined from the

ratio of scattered electron intensities. If we assume that most experimental parameters such as incident electron flux, scattering geometry, angular acceptance, etc are well understood or measured, then the main experimental issue that has to be resolved is usually the determination of the transmission of the energy analysing device (e.g., a hemispherical analyser) as a function of the scattered electron energy.

At high incident energies (>100 eV) it is common for the analyser transmission to be assumed constant, even for relatively tightly bound systems such as the rare gases where the excitation energies are in excess of 10 eV. However, as the incident energy approaches threshold, the ratio of the scattered energies for elastic and inelastic processes can be significant (>20), and some strategy must be adopted for measuring, or estimating, the analyser transmission function in order to obtain accurate absolute cross sections for the inelastic events. A number of possible approaches are discussed in the next section and will be contrasted to the strategy that is used in the present work of employing time-of-flight spectroscopy.

From a theoretical point of view, this energy regime is difficult, because many near-threshold resonance features require accurate, and consistent, descriptions of both the N-electron target and the $(N + 1)$-electron collision problems. In calculations, which are targeted towards accurate results for electron-impact excitation, e.g., for the $n = 2$ and $n = 3$ states of He, this goal can be achieved, to a large extent, by putting more emphasis on the description of the excited (1snl) states than on that of the ground state. Since the excited states are reasonably well described by the 1s orbital of He^+ and slightly modified nl orbitals of H, most theoretical approaches fixed the energy of the lowest excited state $(1s2s)^3S$, or the (weighted) average of the $n = 2$ states, and then ignored the fact that the absolute excitation energy from the ground state is generally too small.

In a comparison with angle-differential DCS ratio measurements such as those reported here, however, such an emphasis on the excited states alone may be problematic, since simultaneously good descriptions of the excited states and the ground state are expected to be important. In addition, one might want to ensure not only a good energy spectrum, but also good oscillator strengths and proper accounts of the dipole polarizability of the target states. To achieve all this simultaneously, it is likely that multi-configuration expansions of the target states as well as coupling to the ionization continuum may be important for a highly accurate theoretical description of the problem. One goal of the present paper is to investigate to what extent this is indeed the case.

In the following sections, we briefly describe the experimental and theoretical techniques that were applied to the problem of near-threshold excitation of the $n = 2, 3$ states of helium. Measurements and calculations of differential scattering cross sections at incident energies of 20.30 eV, 22.00 eV and 23.48 eV are then presented and discussed in section 3 of the paper.

2. Techniques

2.1. Experimental approach

The experiment consists of a crossed electron–helium beam configuration, with the incident electron beam produced from a combination of a thermionic electron source, electrostatic electron optics and a hemispherical monochromator. The energy of the incident beam is readily tuneable and calibrated, in the present case, by measuring well-known resonance features in the metastable atom excitation function (Buckman *et al* 1983). These measurements also indicate that the energy resolution of the incident beam is typically 60–80 meV, with a CW beam current between 5 and 20 nA. The atomic beam is formed by effusive flow of helium through a small, single capillary tube.

The essential new feature of the present experiment is the use of a time-of-flight (ToF) energy analyser as the dispersive element for the scattered electron analysis. Scattered electrons are allowed to drift for 20 cm in a field-free environment before striking a large area position-sensitive detector comprising an 80 mm diameter channel plate and delay-line anode (Röentdek DLD-80). Scattered electrons can be simultaneously detected over a range of scattering angles of about 22° and, by measuring their time-of-flight, their energy can also be determined. The ToF analyser is fixed and the mean scattering angle is varied by changing the position of the electron monochromator, which is mounted on a rotating turntable. As the experiment involves the measurement of electron flight times, a pulsed electron beam is required to initiate the atomic collision. In our case, a pulsed beam of several ns duration (FWHM) is formed by sweeping the beam, in a controlled fashion, across a small defining aperture. Space does not permit a full description of the apparatus here but further details can be found elsewhere (Lange *et al* 2005, 2006). This technique is also similar to the approach of Le Clair *et al* (1996), although in the present case the use of an energy-resolved electron source greatly enhances the sensitivity.

The significant advantages of the ToF technique are that it is multi-channel, with the concomitant efficiency gains and, in the absence of external electric and magnetic fields in the flight region, the transmission between target and detector is independent of the energy of the scattered electrons. Thus in the present apparatus where the flight region is fully enclosed in a conical molybdenum-lined tube, and magnetic fields are less than 1 mG, the ratio of the scattered electron intensities for particular features should be directly proportional to the ratio of the differential scattering cross sections for those features. This differs from other state-of-the-art approaches (e.g. Allan (2005), Khakoo *et al* (2005)), where careful measurements of the analyser transmission were carried out in order to obtain absolute cross sections. Results from the present technique are, however, entirely complementary to these alternate approaches, and offer the opportunity to establish some benchmark standards for near-threshold collision processes.

2.2. Theoretical approaches

All numerical calculations for the present paper were performed based on the framework of the close-coupling formalism. Specifically, we applied the *R*-matrix with the pseudo-states (RMPS) method, a new *B*-spline *R*-matrix (BSR) approach, and finally the convergent close-coupling (CCC) method. A summary of the close-coupling formulation, and the respective numerical implementations in the above three methods, was given by Bartschat *et al* (2004) in the context of e–Mg scattering and hence will not be repeated here. Also, while new calculations were performed for the present work, the essential modifications to previously published descriptions of these methods for e–He collisions are (i) a further increase in the number of coupled states and (ii) a different target description, specifically with respect to the choice of physical and pseudo-states (see below). These modifications, if applicable, will be summarized below, but the interested reader is referred to the original publications for details of the respective methods.

As outlined by Bartschat *et al* (2004), none of the methods directly solves the well-known close-coupling equations in coordinate space, as they can be found in textbooks on quantum collision theory. Both *R*-matrix methods summarized below work in coordinate space, but an expansion of the total (projectile + target) wavefunction, in terms of a suitable basis set to describe the projectile motion inside a box of radius a, is used instead of attempting a more straightforward solution of the resulting integro-differential equations for the projectile wavefunction. The major advantage of the method lies in the fact that, once the basis has

been determined by a *single* diagonalization of the $(N + 1)$-electron Hamiltonian for each partial wave in that box, a large number of collision energies can be treated with a little extra computational effort. The CCC method applied here works in momentum space, directly aiming at the transition matrix elements rather than at solving for the functions of interest in coordinate space and then obtaining these elements through a matching procedure to the known asymptotic behaviour. Since the results are only obtained for one collision energy at a time, a very large number can be coupled without running into numerical instability problems, but the computational resources required are essentially proportional to the number of collision energies dealt with.

It is also worth to briefly discuss the type of N-electron target states used in these close-coupling expansions. Over the past decade, it has been shown on numerous occasions that coupling to the ionization continuum is often absolutely critical in order to obtain reliable theoretical results, especially for optically forbidden transitions at 'intermediate' incident energies, ranging from about one to a few times the ionization threshold. However, even at low energies, and sometimes even for optically allowed transitions, this coupling can be important. All the methods described below account for this coupling via the use of the so-called pseudo-states, i.e., unphysical states generated through pseudo-orbitals, whose relatively short range is comparable to the range of the physical states included in the calculation. These pseudo-states provide a reduced discretization of the infinite number of physical bound Rydberg states as well as the ionization continuum. Coupling to the pseudo-states affects the results for the transitions between the physical states of interest, and it is known to be an effective method to account for the influence of the true bound and continuum states, which cannot be included directly in the close-coupling expansion. Finally, while only the CCC method refers to a 'convergent' expansion already in its name, we note that the RMPS and BSR methods are also convergent in the sense that systematically increasing the number of states in the respective expansions will lead to the same converged result as the CCC if the initial ingredients, essentially the interaction Hamiltonian, are the same. Because of numerical details, however, this may not happen immediately in practice. Most importantly, the number of pseudo-states and their thresholds are usually different. Only with infinite computer power and no numerical instabilities, all three methods should give identical results.

2.2.1. R-matrix with pseudo-states (RMPS) calculations. The details of this calculation were described by Bartschat *et al* (1996) and Hudson *et al* (1996). The principal purpose of presenting results based on work performed 10 years ago is to illustrate to what extent this pioneering RMPS calculation for e–He collisions withstood the test of time. While several more extensive calculations have been performed for this problem since then, we will see that the above model, indeed, contained the essential ingredients to generate highly accurate results for transitions involving the $(1s^2)\ ^1S$ ground state and the lowest four excited states, $(1s2s)\ ^{3,1}S$ and $(1s2p)\ ^{3,1}P$ of helium. In fact, these were the only 5 physical states included in that model, but an additional 36 pseudo-states were generated to improve the target description and to account for the coupling to the higher lying discrete states and the ionization continuum. This model will be referred to as RMPS (5+36) below. Because of the limited number of physical target states in this model, RMPS (5+36) results will only be shown for incident energies of 20.30 eV and 22.00 eV.

2.2.2. B-spline R-matrix (BSR) calculations. Further numerical calculations for the present work were performed with a newly developed computer program (Zatsarinny 2006). It is based upon the B-spline R-matrix approach described, for example, by Zatsarinny and Froese Fischer (2000) and Zatsarinny and Bartschat (2004). The key feature of this approach is to significantly improve the target description by using compact configuration-interaction

expansions involving non-orthogonal sets of term-dependent one-electron orbitals. In helium, specifically, this method allows for the use of various 1s orbitals, which are known to be very different for the $1s^2\,{}^1S$ ground state and essentially all $1snl$ excited states.

As described in detail in a recent publication (Stepanovic *et al* 2006), the target states of helium in the present calculations were generated by combining the multi-configuration Hartree–Fock (MCHF) and the *B*-spline box-based close-coupling (BBCC) methods. The MCHF method (Froese Fischer *et al* 1997) was used for the $1s^2\,{}^1S$ and $1s2l$ states, for which the short-range correlation is known to be very important, while the *B*-spline box-based close-coupling (BBCC) method (Zatsarinny and Froese Fischer 2002) was used for all other excited states.

The BSR scattering model for the present work contained 126 coupled states (BSR126) with S, P, D and F symmetries. All states up to $n = 3$ (11 in total) are well-described physical states (see tables 1 and 2 of Stepanovic *et al* (2006)). The remaining 115 states are pseudo-states, whose principal purpose is to approximate the coupling to the remaining bound states as well as to the ionization continuum (up to a total energy of 65 eV) and also to the $2l2l'$ autoionizing states. Since, in the present work, we are interested in transitions involving only the $n = 2$ and the $(1s3s)^3S$ state, the choice of only having 11 physical states is computationally advantageous. This is of particular importance for *R*-matrix approaches, since the *R*-matrix radius is determined by the range of the physical states. Increasing this radius also increases the number of basis functions needed for a given range of energies and, ultimately, the computer time required to perform such calculations. In the case of Stepanovic *et al* (2006), on the other hand, resonances associated with the physical $n = 4$ and $n = 5$ states were resolved, but at the expense of essentially neglecting the coupling to the continuum.

For the present study, we performed calculations for all scattering symmetries with combined (target + projectile) orbital angular momenta $L \leqslant 25$. For the energies and transitions of interest here, the results are estimated to be converged, within 0.01%, with respect to additional partial waves.

2.2.3. Convergent close-coupling (CCC) calculations. The third theoretical method applied to the problem is the CCC method. The details of the method were given by Fursa and Bray (1995). Briefly, the target states are obtained by diagonalizing the helium Hamiltonian using a Laguerre-based configuration interaction expansion. Typically, all of the target states are obtained sufficiently accurate within the frozen-core approximation, which ensures that one of the two electrons is described by the 1s orbital of He^+. The biggest error is in the ground state ionization threshold (24.6 eV), which is underestimated by 0.84 eV. Accordingly, within the frozen-core approximation we reduce the incident energy by 0.84 eV to ensure that there is as little error as possible in the total energy. By relaxing this approximation we may readily improve the accuracy of the ionization threshold, but it is very rare for the scattering results to be significantly affected. This has been checked to be the case presently, and instead convergence with respect to the size of the expansion of the remaining electron has proved to be more important.

Different energy regimes and different transitions typically involve different convergence considerations. However, for the sake of simplicity, as for the *R*-matrix calculations the CCC results presented here all come from CCC calculations with the same target-state expansion. By taking a total of 87 states (20, 17 and 7 singlet S-, P- and D-states, and 19, 17 and 7 triplet S-, P- and D-states) we believe the presented CCC calculations are sufficiently convergent at all considered energies. States up to $n = 4$ are good eigenstates. Additionally, there is one more negative-energy state for each target symmetry considered, while the rest are positive-energy states.

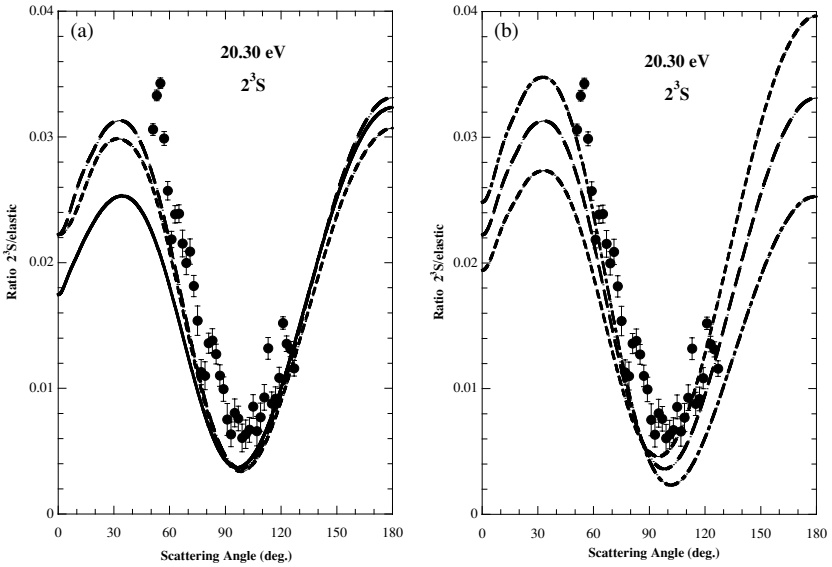

Figure 1. (a) The ratio of the differential cross section for the excitation of the 2^3S state at 20.30 eV to that for elastic scattering: (•) experimental result, (——) CCC calculation, (– – –) RMPS (5+36) calculation, (— — —) BSR126 calculation. (b) A comparison between the (•) experimental ratio and the *B*-spline *R*-matrix calculation at energies of (– – –) 20.25, (— — —) 20.30 and (— · —) 20.35 eV.

3. Results and discussion

Measurements and calculations were carried out at three incident electron energies: 20.30, 22.00 and 23.48 eV. To facilitate the comparison, the data are presented in the raw form in which they are obtained from the experiment, as ratios of the inelastic to elastic scattering intensities. Of course, the absolute inelastic scattering cross sections can be obtained by reference to that for the elastic channel, and some examples of such 'benchmark' cross sections are discussed later. The comparison is made between the experimental results and three variations of the scattering calculations, two using the *R*-matrix formalism and one the convergent close-coupling approach. These various calculations, using the *R*-matrix plus pseudo-states (RMPS (5+36)), *B*-spline *R*-matrix (BSR126) and the convergent close-coupling (CCC) methods, were discussed in the previous section.

At 20.30 eV only one excited channel is open, the 2^3S state, and the excess energy for this state is 0.48 eV. This incident energy also roughly corresponds to the centre of the broad 1s2s2p ^2P negative ion resonance. As this resonance has a width of about 400 meV (Buckman and Clark 1994) and the angle-integrated cross section for the 2^3S state varies rather slowly with an incident energy around 20.30 eV, it was not expected to have any significant effect on the comparison between theory and experiment. However, somewhat surprisingly, all three theories predict a strong energy dependence in the DCS ratio, and this is illustrated in figure 1. In figure 1(a) we show a comparison between experiment and the three calculations at the experimental energy of 20.30 eV. While the three theoretical curves exhibit the same overall angular behaviour, there are differences of 10–20% in the forward and backward scattering directions, and some of these differences are due to differences in the calculated elastic cross sections. The overall agreement with experiment is quite good, although the experimental ratio is consistently about 5–10% higher than that of the largest theoretical value from the *B*-spline

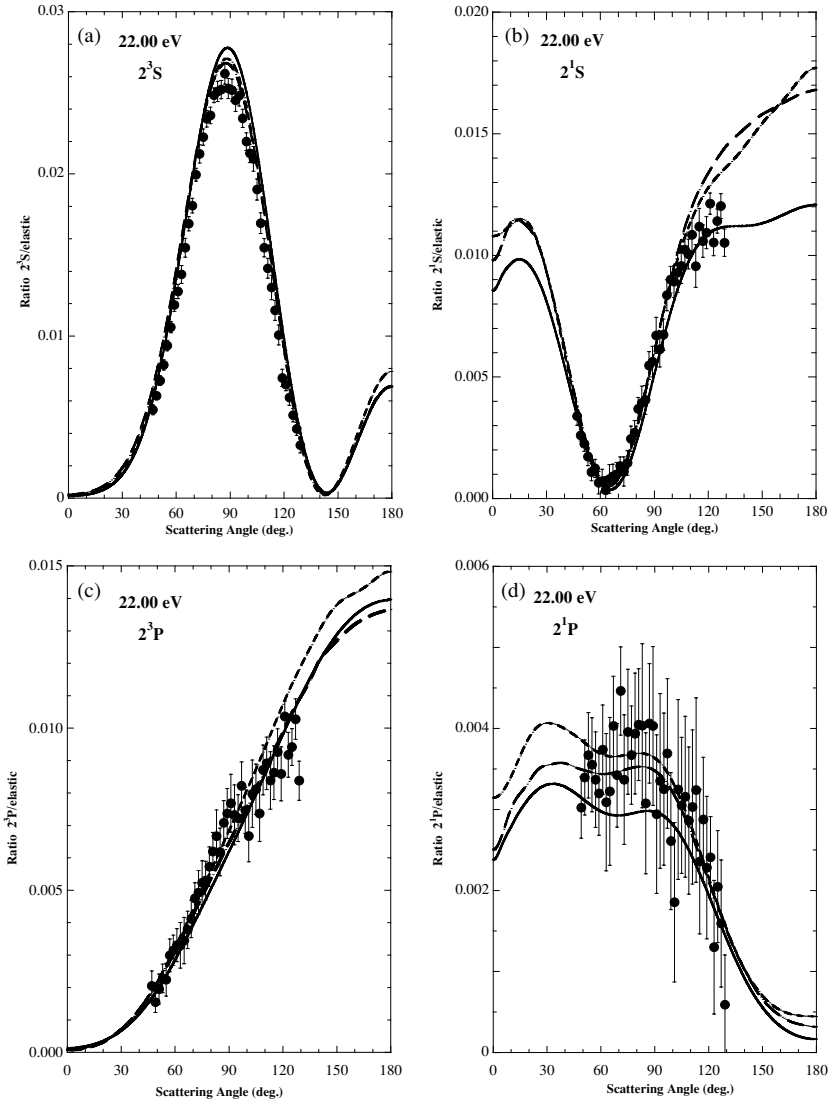

Figure 2. The ratio of the differential cross section for the excitation of the $n = 2$ states of He to that for elastic scattering at an incident energy of 22.00 eV: (a) 2^3S, (b) 2^1S, (c) 2^3P and (d) 2^1P. The key to the data is (•) experimental result, (——) CCC calculation, (– – –) RMPS (5+36) calculation and (— — —) BSR126 calculation.

R-matrix (BSR126) calculation. The difficulty imposed by the strong energy dependence of the DCS ratios is illustrated in figure 1(b) where this energy dependence, no doubt due to the underlying broad shape resonance, is illustrated by two additional BSR126 curves for 20.25 eV and 20.35 eV, respectively.

At 22.00 eV all of the $n = 2$ scattering channels are open and the excess energies involved are 2.18 eV (2^3S), 1.38 eV (2^1S), 1.04 eV (2^3P) and 0.78 eV (2^1P), respectively. The comparisons between the experimental scattering ratios, and those from the various scattering calculations, are made in figures 2(a)–(d), respectively. This energy also represents

a region between the $n = 2$ and $n = 3$ He^- resonances, so the comparison should not be complicated by the presence of underlying resonant features. For the 2^3S state (figure 2(a)), the agreement between experiment and theory is excellent, in both angular dependence and magnitude. While, for the sake of clarity, we do not show them in the figure, the earlier experimental results of Asmis and Allan (1997) at this energy are also in excellent agreement with the present experiment. A similar excellent level of agreement is seen for the 2^1S state (figure 2(b)). Differences in the theoretical ratios emerge at angles above about 100°, with both *R*-matrix approaches predicting a larger ratio than the CCC. Although the overlap between experiment and theory in this large-angle range is small, there would appear a marginally better agreement between the experiment and the CCC calculation above 100°. For the 2^3P state (figure 2(c)) the agreement between experiment and all three calculations is very good at all angles. For the 2^1P state (figure 2(d)), the cross-section ratio is quite small, reflecting the small inelastic cross section at this near-threshold energy. All three calculations exhibit the same general angular behaviour, but there are differences in magnitude in some cases of ∼25%. However, the uncertainties on the experimental ratios are quite large for this channel and it is not really possible to draw any solid conclusions from the comparison, other than that there is good general agreement between experiment and theory.

At 23.48 eV, the situation is somewhat more complicated in that this energy corresponds to a region where a number of sharp, doubly excited He^- resonance features are located. In particular, the $1s4s^2\ ^2S$ and $1s4s4p\ ^2P$ configurations, at 23.44 eV and 23.52 eV, respectively (Buckman *et al* 1983, Stepanovic *et al* 2006), may be excited by the relatively broad energy profile of the incident electron beam. Nonetheless the comparison between experiment and theory in figures 3(a)–(d) is still useful and, once again, quite encouraging. At this incident energy the excess energies for the $n = 2$ excited states are 3.66 eV (2^3S), 2.86 eV (2^1S), 2.52 eV (2^3P) and 2.26 eV (2^1P). We have also investigated the excitation of the 3^3S state, and the excess energy for this channel is 0.76 eV.

Given the overlap with the sharp negative-ion features at this energy, and the broad energy width (∼100 meV) and uncertainty of the absolute energy (∼30 meV) in the experiment, we also investigated the effect of small shifts of the incident energy on the calculated ratios. The BSR126 calculations were carried out at incident energies of 23.45, 23.48, 23.50 and 23.55 eV. In a few cases the differences between the calculated ratios across this energy span were significant (>50%), particularly for the 2^3P and 2^1P states, and in many cases they were of the order of 10–20%. This simply reflects the rapidly changing resonance phaseshifts and profiles. The CCC calculations showed remarkably similar energy dependence. As a result we have chosen to compare with the BSR126 and CCC predictions at the experimental energy of 23.48 eV, but also to show a comparison with the BSR126 calculation at 23.50 eV, in order to illustrate the effect that a small energy shift of only 20 meV can produce. The experimental and theoretical results are shown in figures 3(a)–(e).

For the 2^3S state (figure 3(a)) the two theoretical predictions are in good agreement with each other, and both are higher than experiment, particularly at intermediate scattering angles. The BSR126 calculation at 23.50 eV is in much better agreement with experiment at all angles. For the 2^1S state (figure 3(b)), the agreement between experiment and theory is excellent and we see that there is also little difference between the theories themselves, or the BSR calculation at different energies, with the exception of the region of very large scattering angles. For the 2^3P state (figure 3(c)), the BSR126 and CCC calculations are in excellent agreement with one another. The experiment lies uniformly lower than the theory, by about 5–10%, for angles up to about 100°. Beyond that, the experimental cross section turns over, while both calculations rise to a maximum value at 180°. The BSR126 calculation at 23.50 eV is not significantly different at lower scattering angles, but it shows similar behaviour

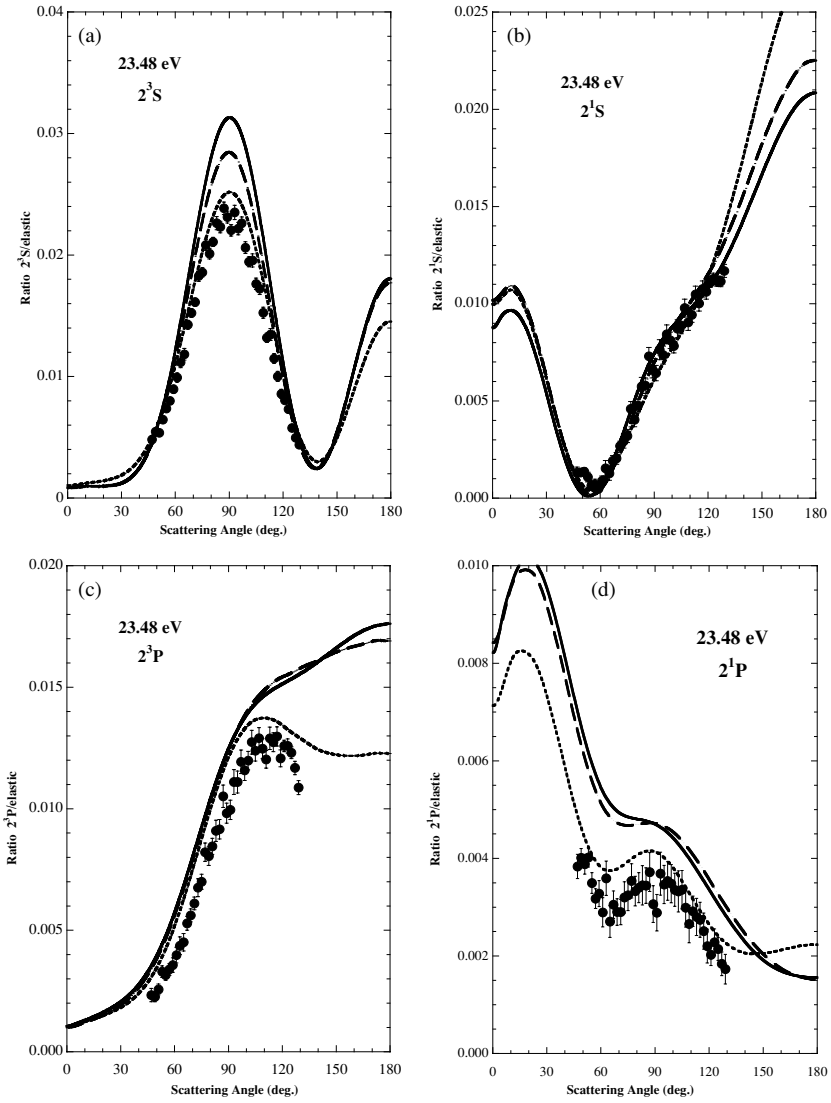

Figure 3. The ratio of the differential cross section for the excitation of the $n = 2$ states of He to that for elastic scattering at an incident energy of 23.48 eV: (a) 2^3S, (b) 2^1S, (c) 2^3P, (d) 2^1P and (e) 3^3S. The key to the data is (•) experimental result, (——) CCC calculation, (— — —) BSR126 calculation at 23.48 eV and (- - - -) BSR126 calculation at 23.50 eV.

to experiment above 90°, and is certainly closer to the experimental cross-section ratio at larger angles. In figure 3(d) we show the ratios for the 2^1P state in comparison with the two theoretical techniques. The CCC and BSR126 calculations are in excellent agreement and show a similar angular dependence as the experiment, although they are about 30–50% higher. On the other hand, the BSR126 calculation, at the higher energy of 23.50 eV, is in better agreement with experiment.

Finally, at 23.48 eV, we show the comparison between experiment and theory for the cross-section ratio for the 3^3S state (figure 3(e)). Once again the same general angular dependence

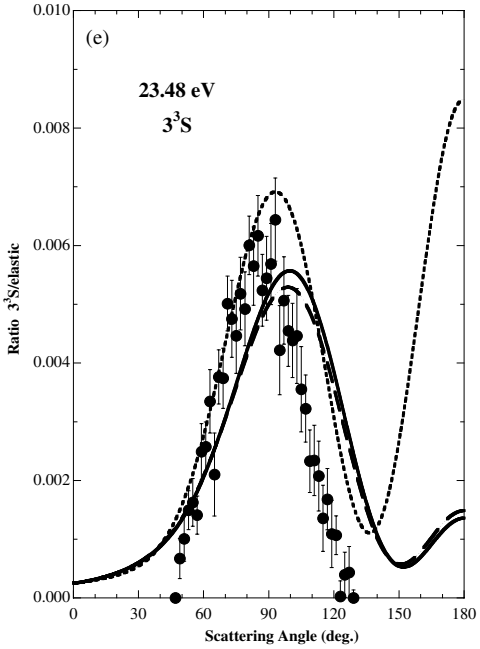

Figure 3. (Continued.)

Table 1. Recommended differential cross sections (in units of 10^{-19} cm^2 sr^{-1}) for the electron impact excitation of several of the $n = 2$ states of He at a number of incident energies and scattering angles. We estimate that these values are accurate to within ∼10%.

Energy (eV)	2^3S	2^1S	2^3P
20.3	1.98 at 120°	–	–
22.0	4.67 at 90°	1.48 at 100°	1.75 at 120°
23.48	–	1.77 at 120°	–

is observed in both theory and experiment, and it also looks quite similar to that for the 2^3S state (figure 3(a)). The CCC and BSR126 calculations are in excellent agreement with each other but show some differences from the experiment. Once again, the BSR126 calculation at the slightly higher energy of 23.50 eV is in better agreement with experiment.

Given the excellent agreement, at some energies and angles between experiment and theory, it is possible for us to suggest some 'benchmark' cross-section values for the various excited states. These values are provided in table 1 and we estimate that the uncertainty on these values should not be more than ±10%. They could be useful, for example, for the cross calibration of other electrostatic electron spectrometers used for near-threshold excitation measurements, or for benchmarking comparisons with other theoretical calculations.

4. Conclusions

A new experimental technique for angle-differential, near-threshold electron impact excitation of atoms and molecules has been demonstrated through a series of measurements for the $n = 2$, 3 excited states of helium. This technique employs temporal energy dispersion of

all scattered electrons in a field-free environment and reveals energy and angular spectra, where the ratios of the peak intensities for each scattering channel, elastic and inelastic, should be proportional to their differential scattering cross sections. While the energy range of the technique is limited to the region immediately above (within ∼10 eV) the excited state thresholds, it has the ability to provide ratios of elastic to inelastic scattering, which are independent of the transmission of the analyser, which should be uniform as a function of energy. In this way absolute differential scattering cross sections (DCS) for the inelastic processes can be obtained from knowledge of the elastic DCS.

Measurements, at a few selected energies, of the inelastic-to-elastic scattering ratios have been compared with the state-of-the-art theory, and the agreement is generally very good. This indicates that the essential physics, i.e., the target description and the channel coupling between the relevant discrete states and the target continuum, are well described in all three theoretical approaches used in the present work. The remaining discrepancies between theory and experiment are most likely due to the calibration of the incident electron energy in the experiment, and the effect of the energy width of the incident beam. This is particularly the case at those incident energies (20.30 eV and 23.48 eV) where sharp, negative-ion resonance features may affect the comparison. Indeed, a careful comparison between experiment and theory indicates that the incident electron energy, particularly in the case of the measurements at '23.48 eV', may actually be higher by about 20 meV than the experimental calibration indicates.

In addition to the comparison of experimental and theoretical scattering ratios, we have generated suggested 'benchmark' cross sections for several of the excited states at a number of incident energies where there is excellent and uniform agreement between experiment and theory.

Acknowledgments

The experimental and theoretical aspects of this work, at the ANU, and at Murdoch University, have been supported by the Australian Research Council and the Deutsche Forschungsgemeinschaft. IB and DF are also grateful to ISA Technologies, Perth, Western Australia, for provision of access to their IBM P690 computer in support of this project. The work at Drake University is supported by the United States National Science Foundation under grants PHY-0244470, PHY-0311161 and PHY-0555226.

References

Allan M 2005 *J. Phys. B: At. Mol. Opt. Phys.* **38** 1679
Asmis K and Allan M 1997 *J. Phys. B: At. Mol. Opt. Phys.* **30** 1961
Bartschat K, Hudson E T, Scott M P, Burke P G and Burke V M 1996 *Phys. Rev.* A **54** R998
Bartschat K, Zatsarinny O, Bray I, Fursa D V and Stelbovics A T 2004 *J. Phys. B: At. Mol. Opt. Phys.* **37** 2617
Brunger M J and Buckman S J 2002 *Phys. Rep.* **357** 215
Buckman S J and Clark C W 1994 *Rev. Mod. Phys.* **66** 539
Buckman S J, Hammond P J, Read F H and King G C 1983 *J. Phys. B: At. Mol. Phys.* **16** 4039
Burke V M and Noble C J 1995 *Comput. Phys. Commun.* **85** 471
Froese Fischer C, Brage T and Jönsson P 1997 *Computational Atomic Structure: An MCHF Approach* (Bristol: Institute of Physics Publishing)
Fursa D V and Bray I 1995 *Phys. Rev.* A **52** 1279
Hudson E T, Bartschat K, Scott M P, Burke P G and Burke V M 1996 *J. Phys. B: At. Mol. Opt. Phys.* **29** 5513
Khakoo M A, Johnson P V, Ozkay I, Yan P, Trajmar S and Kanik I 2005 *Phys. Rev.* A **71** 062703
Lange M, Matsumoto J, Lower J C A, Newman D S and Buckman S J 2006 in preparation

Lange M, Matsumoto J, Setiawan A, Lower J C A and Buckman S J 2005 *J. Electron Spectrosc. Relat. Phenom.* **144–147** 993

Le Clair L R, Trajmar S, Khakoo M A and Nickel J C 1996 *Rev. Sci. Instrum.* **67** 1753

Stepanovic M, Minic M, Cvejanovic D, Jureta J, Kurepa J, Cvejanovic S, Zatsarinny O and Bartschat K 2006 *J. Phys. B: At. Mol. Opt. Phys.* **39** 1547

Zatsarinny O 2006 *Comput. Phys. Commun.* **174** 273

Zatsarinny O and Bartschat K 2004 *J. Phys. B: At. Mol. Opt. Phys.* **37** 2173

Zatsarinny O and Froese Fischer C 2000 *J. Phys. B: At. Mol. Opt. Phys.* **33** 313

Zatsarinny O and Froese Fischer C 2002 *J. Phys. B: At. Mol. Opt. Phys.* **35** 4669